ADVANCED ENERGY MATERIALS
www.advenergymat.de

In Situ Topological Interphases Boosting Stable Solid-State Lithium Metal Batteries

Hantao Xu, Jianyong Zhang, Hong Zhang, Juncai Long, Lin Xu, and Liqiang Mai**

Incompatible interphases resulting from the irreconcilable contradiction between impedance and mechanical strength have become one of the major obstacles to the practical application of solid-state lithium metal batteries (SSLMBs). With the employment of a decoupling strategy by rational topological design, herein a topological polymer-reinforced interphase layer is in situ constructed using a synthesized solid polymer electrolyte. As a result, the constructed topological solid electrolyte interphase (SEI) layer harmonizes the enhanced mechanochemical stability and fast diffusion dynamics of Li^+, which maintains the integrity and stability of the SEI layer during cycling. In addition, a highly stable and reversible Li nucleation/stripping behaviors exceeding 3000 h and the superior cycling performance of practical $LiFePO_4$/Li metal battery beyond 500 cycles can be achieved by virtue of the formation of the topological interphase layer. This design strategy of constructing a topological interphase layer to decouple mechanical strength and the activation energy of Li^+ transport provides a feasible paradigm for realizing practical SSLMBs.

1. Introduction

Solid-state batteries are considered as one of the most promising alternatives to these traditional commercial batteries because of their enhanced safety and higher energy density especially when coupled with lithium metal anodes (LMAs).[1] However, the practical applications of solid-state lithium metal batteries (SSLMBs) are still severely limited by the short lifespans and potential safety hazards, which are mainly caused by the exacerbated parasitic reactions and uncontrollable growth of "dead Li" at the interfaces between solid state electrolytes (SSEs) and the anodes.[2] The origins of these issues are the generation of thermodynamically unstable interface and inhomogeneous plating/stripping of lithium due to high impedance at the solid electrolyte interphase (SEI), scattered distributions of space charge and volume change of lithium anode during cycling.[3] This unstable SEI generally consisting of inorganic and small organic chemicals generated by SSEs is commonly of high impedance and fragile, and can hardly accommodate the vast volume deformation of LMAs during cycling.[4] Eventually, the resulting inhomogeneous stress distribution leads to continuous cracking of undesirable mechanical SEI layer onto the LMA.[5] The propagation of cracks and regenerations of SEI layers continuously expose active sites for interfacial side reactions and the penetration of lithium dendrites, which increase interfacial impedance inside batteries and risks of thermal runaway.[6]

It is of significance to construct mechanically stable and chemically compatible SEI layers for stabilizing the interphase of high safety and high performance SSLMBs.[2b,7] Therefore, some efforts such as the employment of a double-layer solid polymer electrolyte[8] and the addition of inorganic additive with interfacial stability,[9] have been devoted to tackling the issues of the interfacial instability or inferior mechanical strength between SSEs and anodes. Nevertheless, traditional protection strategies cannot reconcile the contradiction between mechanical strength and the activation energy of lithium ion (Li^+) transport. For example, SSEs of polymers with large molecular weight or excessive crosslinking tend to generate SEIs with high mechanical strength but poor interfacial contact (**Figure 1**a), while SSEs of linear polymers with small molecular weight tend to generate polymer-rich SEIs with good ability of Li^+ transport but poor mechanical strength (Figure 1b).[10] In order to modulate uniform lithium nucleation through enhancing desolvation and transport kinetics of Li^+ during the repeated processes of Li deposition on the surface of anodes, it is necessary to build a stable SEI layer with low activation energy of Li^+ transport.[4a,11]

Poly(1,3-dioxolane)-based (PDOL-based) quasi-solid-state electrolytes have been widely reported for their high conductivity and excellent cycling performance.[12] However, in order to prepare solid-state PDOL-based batteries with higher safety, the problems

H. Xu, J. Zhang, H. Zhang, J. Long, L. Xu, L. Mai
State Key Laboratory of Advanced Technology for Materials Synthesis and Processing
School of Materials Science and Engineering
Wuhan University of Technology
Wuhan 430070, P. R. China
E-mail: linxu@whut.edu.cn; mlq518@whut.edu.cn

L. Xu, L. Mai
Hubei Longzhong Laboratory
Wuhan University of Technology (Xiangyang Demonstration Zone)
Xiangyang, Hubei 441000, P. R. China

L. Xu, L. Mai
Hainan Institute
Wuhan University of Technology
Sanya 572000, P. R. China

The ORCID identification number(s) for the author(s) of this article can be found under https://doi.org/10.1002/aenm.202204411

DOI: 10.1002/aenm.202204411

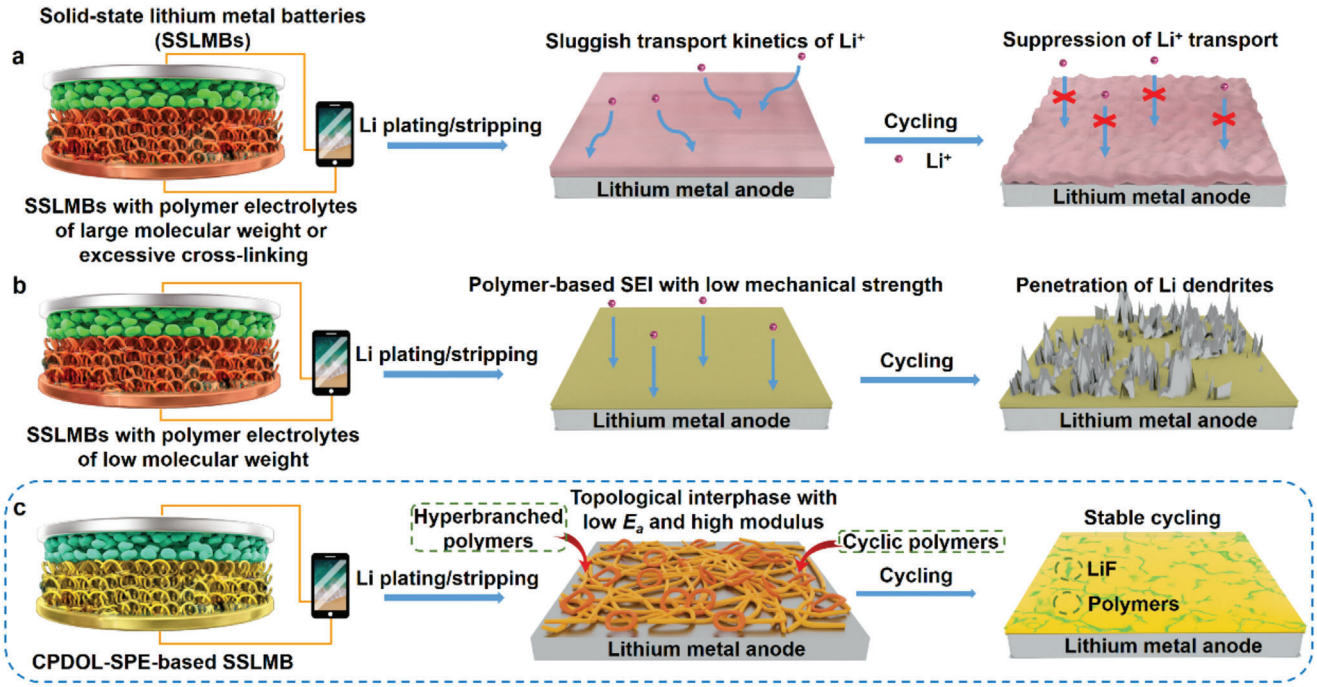

Figure 1. Schematic diagram of in situ generation of varied solid electrolyte interphases (SEIs) in solid-state lithium metal batteries (SSLMBs). a) SEI with high impedance. b) SEI with low mechanical strength. c) Topological interphase.

of low mechanical strength and poor interfacial compatibility at the solid-solid interphase cannot be ignored, which can lead to performance degradation and even cause safety hazards.[13] Rational high-entropy topological design can decouple the mechanical strength and the mobility of ions in polymers, thus improving the mechanochemical stability of the polymer electrolytes and reducing the activation energy of Li^+ transport of electrolytes.[10] However, few studies have reported the effect of the construction of topological polymer-reinforced interphases on the performance of SSLMBs. In this work, a topological interphase layer is in situ constructed with a synthesized topologically cross-linked poly(1,3-dioxolane)-based solid-polymer-electrolyte (CPDOL-SPE). Experimental and theoretical studies indicate that CPDOL-SPE experiences mild redox reaction with LMA, and then in situ constructs a topological interphase layer with topological polymers of cyclic and hyperbranched structures that can reconcile high mechanochemical stability and fast transport kinetics of Li^+ (Figure 1c). In addition, the topological interphase layer modulates the aggregation of $TFSI^-$ anions through supramolecular hydrogen bonding interactions between −NH and −F, and thus makes it participate in the construction of a topological polymer-reinforced LiF-rich SEI layer. Therefore, this SEI layer exhibits low impedance of charge transfer, suppression of lithium dendrite penetration and cracks of SEI, and effective prohibition of further side reactions between the CPDOL-SPE and LMA. As a result, the topological interphase layer induced by CPDOL-SPE achieves an extremely stable Li/Li cycling performance beyond 3000 h and long-life SSLMB exceeding 500 cycles with $LiFePO_4$ cathode and practical LMA. This study inspires the optimal design of SEI layers toward practical realization of high-performance and long-life CPDOL-SPE-based SSLMBs.

2. Results and Discussion

2.1. Preparation and Characterizations of the As-Developed CPDOL-SPE

The block precursor of topological CPDOL-SPE, named poly(1,3-dioxolane) urethane dimethacrylate (PDOLUDMA), is synthesized by a two-step reaction (Figure S1, Supporting Information, Experimental Section). The sharp peaks of $-CH_3$ and C=C appear completely (**Figure 2**a), indicating the successful synthesis of precursor PDOLUDMA. Fourier transform infrared spectroscopy (FTIR) analysis illustrates that the stretching vibration absorption peak located at ≈1626 cm^{-1} of C=C almost disappears after polymerization to CPDOL (Figure 2b), which can be attributed to the high conversion rate of polymerization from PDOLUDMA to CPDOL.[4a] After the preparation of solid polymer electrolyte membrane with LiTFSI using casting method, CPDOL-SPE exhibits a top view of smooth and compact (Figure S2, Supporting Information). Cross-sectional scanning electron microscope (SEM) image of the membrane of CPDOL-SPE shows that the thickness of the prepared ultra-thin membrane is ≈16 µm (Figure 2c). Optical photo of CPDOL-SPE-based membrane shows the properties of ultrathin, colorless and high transparency (Figure 2d). The result of matrix-assisted laser desorption/ionization time of flight mass spectrometry (MALDI-TOF-MS) indicates the presence of topological polymers with cyclic and hyperbranched structures in the synthesized CPDOL polymers (Figure S3, Supporting Information). Gel permeation chromatography indicates that the average molecular weight (Mw) of PDOL, PDOLUDMA, and CPDOL are about 2.5×10^4, 2.8×10^4, and 1.1×10^5 g mol^{-1}, respectively, proving successful synthesis of topological CPDOL (Figure S4, Supporting Information).

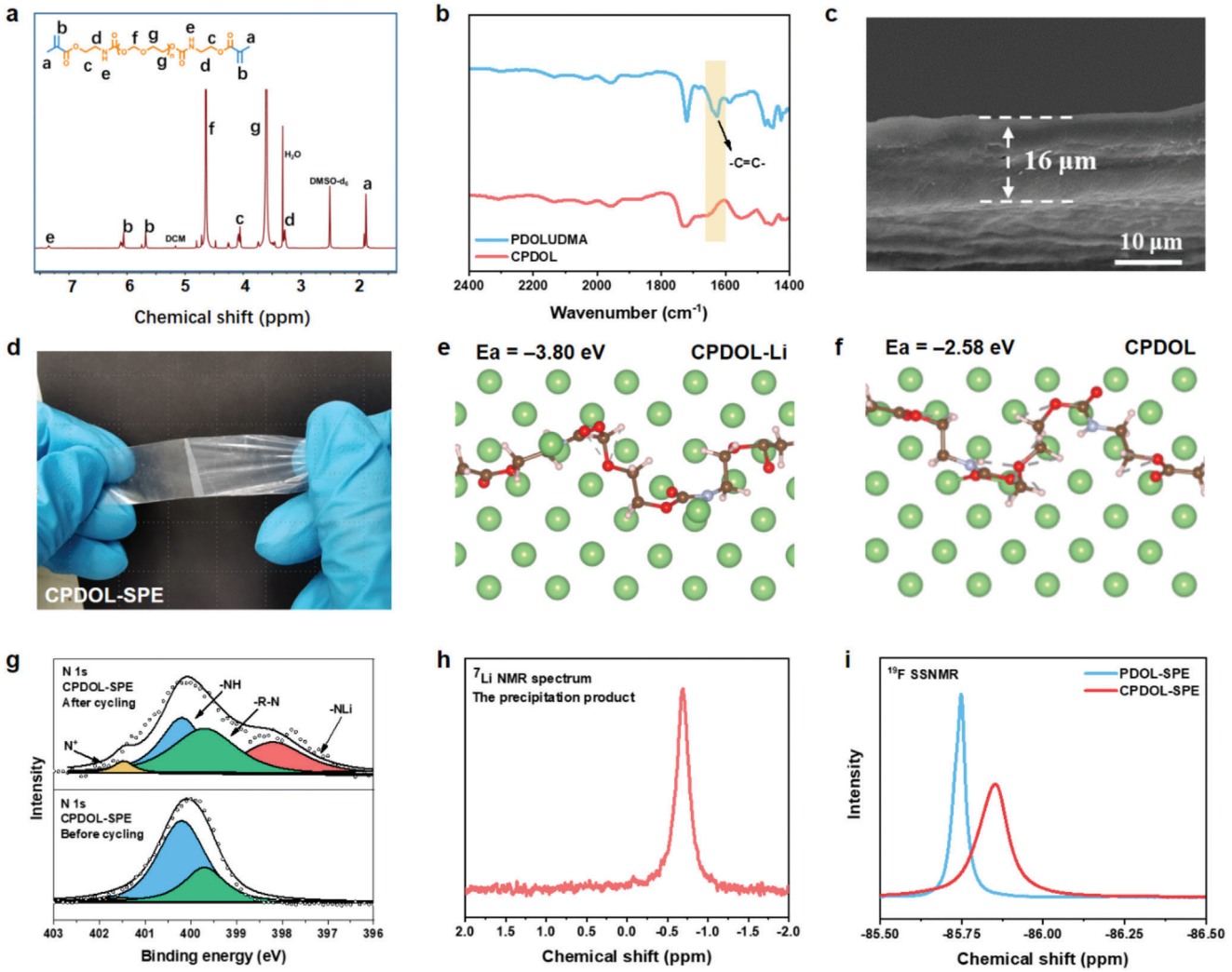

Figure 2. Characterizations of topological polymers and solid electrolytes. a) ^{1}H NMR of poly(1,3-dioxolane) urethane dimethacrylate (PDOLUDMA) precursor. b) FTIR spectra of CPDOL and PDOLUDMA. c) Cross-section view of cross-linked poly(1,3-dioxolane)-based solid-polymer-electrolyte (CPDOL-SPE). d) Top-view of optical photograph of CPDOL-SPE. e) DFT calculation model and the as-obtained adsorption energy of CPDOL. f) DFT calculation model and the as-obtained adsorption energy of CPDOL-Li. g) XPS N 1s spectra of the surface of CPDOL-SPE before and after 10 cycles. h) ^{7}Li NMR of the precipitation products of CPDOL-SPE after cycling. i) ^{19}F solid-state nuclear magnetic resonance (SSNMR) of PDOL-SPE and CPDOL-SPE after 10 cycles.

Moderate cross-linking degree of topological polymer can improve both mechanical properties and the ability of ionic migration.[10] Owing to the reduced crystallinity brought by the introduction of the cross-linked structure from urethane dimethacrylate motif and intermolecular interactions, it is demonstrated that the T_g point of CPDOL-SPE (−45.86 °C) is slightly lower than the T_g point of PDOL-SPE (−44.15 °C). It indicates that CPDOL-SPE has high segment mobility, which can effectively promote the migration of Li^+ in the electrolyte, delivering better ionic conductivity (Figure S5, Supporting Information). AC impedance test results show that the optimal LiTFSI concentration is 40 wt% (Figure S6, Supporting Information). Moreover, CPDOL-SPE delivers a relatively high ionic conductivity of 1.01×10^{-4} S cm^{-1} at operating temperature (Figure S7, Supporting Information) with a low level of activation energy (E_a) (E_a = 0.21 eV) (Figure S8, Supporting Information). Linear sweep voltammogram (LSV) measurement indicates that the as-investigated CPDOL-SPE exhibits a slightly higher oxidation decomposition potential (5.1 V versus Li/Li^+) than that of the PDOL-SPE (Figure S9, Supporting Information). The results of electrochemical floating analysis show that no leakage current is observed in CPDOL-SPE (<10 μA) at voltages below 5.0 V (Figure S10, Supporting Information). In contrast, the instable leakage current of PDOL-SPE measured at 5.0 V proves the anodic instability of PDOL-SPE, which is consistent with the result of LSV curve. Such a high oxidation-resistant ability of the as-developed CPDOL-SPE can be ascribed to the lower highest occupied molecular orbital (HOMO) energy of CPDOL than PDOL (Table S1, Supporting Information). In addition, CPDOL-SPE delivers an enhanced lithium ion transference number (t_{Li}^+) of 0.46 (Figure S11a,b, Supporting Information), higher than that (t_{Li}^+ = 0.32) of PDOL-SPE (Figure S11c,d, Supporting

Information), commercial liquid electrolyte (≈0.4)[14] and PEO-based-SPE (≈0.2).[15] Such an enhanced t_{Li}^+ of CPDOL-SPE can be attributed to the fast segmental movement kinetics of CPDOL segments and intermolecular interactions between urethane motifs and $TFSI^-$ anions, which slowed the movement of anions. According to the "space charge model", the "sand time" as the time of dendrite growth is heavily influenced by the t_{Li}^+.[16] Hence, the superior t_{Li}^+ of CPDOL-SPE helps reduce the lithium polarization by inhibiting the formation of a concentration gradient, and regulates Li nucleation behaviors. These results suggest that the CPDOL-SPE delivers enhanced electrochemical properties such as high ionic conductivity, high anodic stability, and high t_{Li}^+ exhibiting good potential for battery applications.

2.2. Characterizations of Topological Interphase Layers

CPDOL-SPE tends to in situ generate a topological interphase layer of CPDOL-Li derivative during cycling owing to the in situ redox reaction between LMA and the active hydrogen on urethane group (Figure 1c and Figure S12, Supporting Information).[17] To demonstrate this mechanism, the energy levels of the lowest unoccupied molecular orbital (LUMO) of the polymer matrixes were calculated. The results of simulation show that the LUMO of CPDOL (0.109 eV) is significantly lower than that of linear PDOL (0.834 eV), indicating that CPDOL is more likely to react with the LMA and form a topological CPDOL-based SEI (Table S1, Supporting Information). Furthermore, differential charge densities and electrostatic potential maps of polymer fragments were calculated. In the reaction of CPDOL structure with lithium metal, α-hydrogen on urethane segment has a high tendency of electron aggregation, which means that the electron lost from lithium metal will be preferentially transferred to α-hydrogen to balance the Fermi level, and thus α-hydrogen will be replaced by Li (Figures S13 and S14a, Supporting Information).[18] The adsorption energy (−3.8 eV, Figure 2e) of generated CPDOL-Li with Li is much lower than that of CPDOL (−2.58 eV, Figure 2f), indicating that Li metal is inclined to adsorb CPDOL-Li, which subsequently participate in forming a polymer-reinforced topological SEI layer. In addition, less electron transfer to CPDOL-Li occurs on the surface of lithium metal (Figure S14b, Supporting Information), which indicates that the structure of CPDOL-Li is more stable on the surface of lithium metal compared to CPDOL (Figure S14a, Supporting Information).[19]

To experimentally demonstrate the generation of this topological interphase composed of CPDOL-Li, as-prepared CPDOL-SPEs after 10 cycles were characterized. For instance, FTIR spectrum exhibits that a new C=O peak at 1648 cm^{-1} is enhanced and the original C=O peak disappears on the surface of CPDOL-SPE, which means the chemical environment next to C=O has changed (Figure S15, Supporting Information).[20] X-ray photoelectron spectroscopy (XPS) N1s spectra analysis reveals that the peak of –NLi (≈398.3 eV) and N^+ (401.5 eV) reaction intermediate appear and –NH (≈400.1 eV) weakens on the surface of CPDOL-based interphase after cycles (Figure 2g), indicating that the change in chemical environment is the partial conversion of –NLi from –NH on the polymer structure.[4a,17,21] In addition, in the ^{7}Li nuclear magnetic resonance spectroscopy (NMR) spectrum of precipitated products of CPDOL-SPE after cycling, a peak located at −0.68 ppm corresponding to –NLi is found (Figure 2h), which proves the generation of topological interphase with CPDOL-Li.[4a]

To further reveal the structure of the formed topological interphase, XPS sputtering at different depths on the surface of LMAs were used. In detail, there are much –NH, –NLi, and alkyl N on the surface of interphase, while the composition of N almost disappearing after 3 min sputtering, leaving only a small amount of –NLi component at the bottom of interphase, indicating that the residual –NH is mainly distributed at the upper part of the interphase, while the generated –NLi is distributed at the full depth of the interphase in the vertical structure of topological CPDOL-Li-based interphase (Figure S16a, Supporting Information). For comparison, PDOL-based LMA after 10 cycles is also characterized. Only a small amounts of alkyl N and −NLi that comes from the decomposition of lithium salts in PDOL-based SEI are observed, which is in stark contrast to that of CPDOL-based SEI after cycles (Figure S17, Supporting Information).

Furthermore, XPS F 1s spectra reveal that –CF disappears in the bottom of CPDOL-based SEI, while the content of LiF component is still very high after 3 min sputtering (Figure S16b, Supporting Information), demonstrating that LiF is uniformly distributed in the whole SEI. In order to further investigate the vertical structure of the topological interphase layer and verify the chemical structure of the topological polymer-reinforced interphase layer, the deep product of SEI is taken after scraping off the surface component on the surface of LMA. ^{1}H NMR shows that amino α-hydrogen with a broad peak of 7.3 ppm chemical shift is almost absent in the deep SEI after cycling, proving that most of the –NH on the deep layer of the interphase has been converted to −NLi after initial cycling (Figure S18a, Supporting Information). In addition, the polymer structure in the interphase layer is essentially the same as that of CPDOL before cycling, which is confirmed by ^{1}H NMR, proving that the main component of topological polymer-reinforced interphase layer is CPDOL-Li (Figure S18b, Supporting Information). The above results confirm that topological interphase with layered structure of topological CPDOL-Li and LiF is formed after initial cycling.

To demonstrate the source of LiF generation, FTIR spectroscopy at variable temperatures and solid-state nuclear magnetic resonance (SSNMR) were used to analyze intermolecular interactions during cycling. With the increase of temperature from 30 °C to 80 °C, the band located at 3571 cm^{-1} assigned to the −N−H bond shows a gradual blue shift and decreased peak intensity, proving the possible existence of hydrogen bonding (Figure S19, Supporting Information). Besides, SSNMR F 1s spectrum shows the peak of LiTFSI moves downfield and becomes wider after cycles, which confirm that the supramolecular hydrogen bond in the electrolyte is mainly between –NH and LiTFSI (Figure 2i). Hence, this topological interphase can modulate the formation of highly concentrated $TFSI^-$ on the surface of LMA by hydrogen bonding and then uniformly distribute the formed LiF components throughout the interphase.

Enhancing the charge and discharge performance of SSLMBs requires improving the diffusion kinetics of Li^+ at SEI. Rational topology design of the interphase can effectively increase Li^+ diffusion and modulate the uniform deposition of Li^+. From Tafel curves, the calculated value of exchange current density (i_0) in topological CPDOL-based SEI (i_0 = 0.069 mA cm^{-2}) is

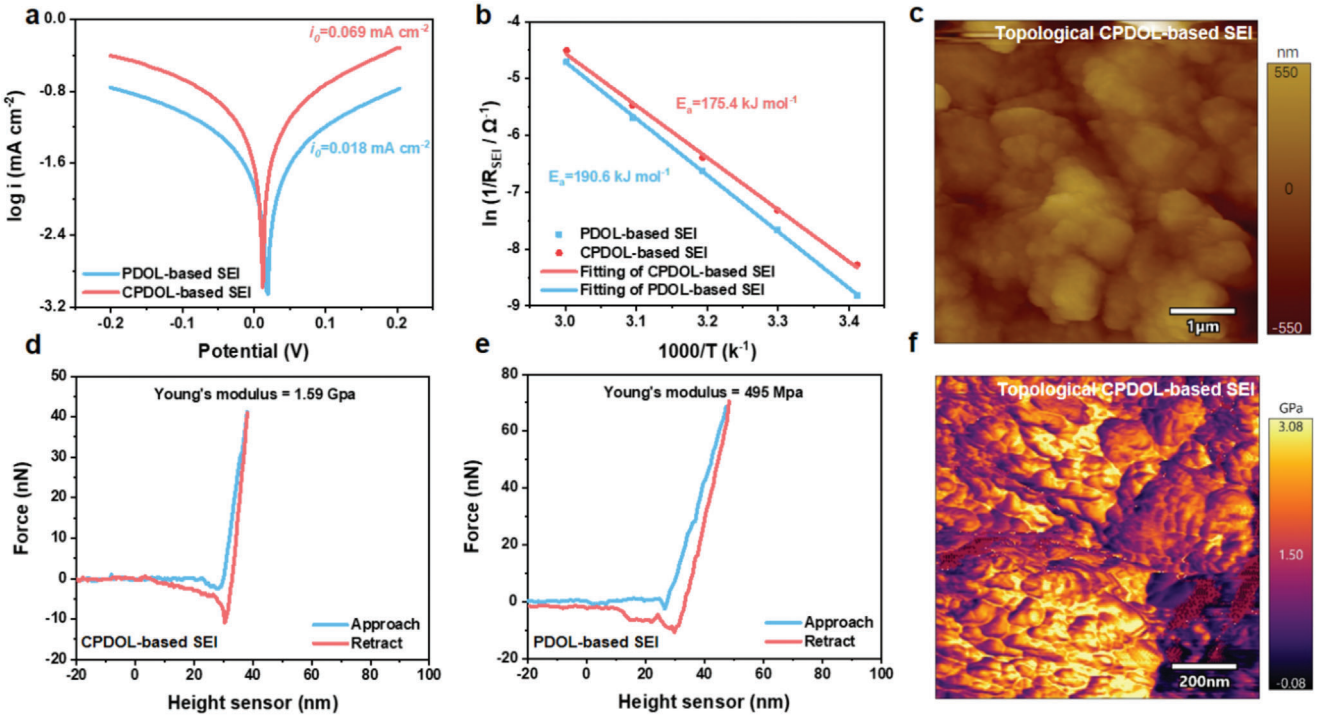

Figure 3. Characterizations of topological interphase layers. a) Tafel plots of cross-linked poly(1,3-dioxolane)-based solid-polymer-electrolyte (CPDOL-SPE) and PDOL-SPE after 10 cycles and the corresponding exchange current density. b) The activation energies for ion diffusion through solid electrolyte interphase (SEI) in various temperatures by Arrhenius equation. c) Vacuum atomic force microscopy (VAFM) height image of topological CPDOL-based SEI. d) Force–displacement curves for nanoindentation experiments for topological CPDOL-based SEI. e) Force–displacement curves for nanoindentation experiments for PDOL-based SEI. f) Surface map of Young's modulus of topological CPDOL-based SEI.

much larger than that in PDOL-based SEI (i_0 = 0.018 mA cm^{-2}) (**Figure 3**a). Meanwhile, the activation energy levels (E_a) of transport of Li^+ in variable SEIs are also calculated. The results show that the topological CPDOL-based SEI has a low E_a of 175.4 kJ mol^{-1}, while the SEI formed in PDOL-SPE has a larger activation energy of 190.6 kJ mol^{-1} (Figure 3b, Table S2, Supporting Information). The lower E_a indicates that the topological interphase in CPDOL-based SSLMB improves the mobility of polymer chains and the free volume, thus enhancing the diffusion kinetics of Li^+, which is more conducive to transport of Li^+.

It was reported that if the SEI is not robust enough to endure the change of volume during the process of Li deposition, the dendrites and "dead Li" are easier to form at the areas of weak mechanical strength.[22] Local mechanical properties of SEIs on the surface of LMAs were measured by nanoindentation using vacuum atomic force microscopy (VAFM). VAFM images show that the surface of CPDOL-based SEI is much smoother than PDOL-based SEI, indicating that the topological SEI with low activation energy is more favorable for the uniform deposition of Li^+ (Figure 3c and Figure S20, Supporting Information). Typical force–displacement curves for nanoindentation experiments on both topological CPDOL-based SEI and PDOL-based SEI are also characterized (Figure 3d,e). The force–displacement curve of topological CPDOL-based SEI during loading and unloading is more reversible than PDOL-based SEI, demonstrating that PDOL-based SEI exhibits an elastic-plastic deformation while the characteristic of topological CPDOL-based SEI is close to elastic deformation with high reversibility. Furthermore, topological CPDOL-based SEI exhibits higher and uniform Young's modulus (1.59 GPa) than PDOL-based SEI (0.49 GPa) (Figure 3d–f and Figure S21, Supporting Information). In order to investigate the source of enhanced mechanical strength, quantitative analysis of elements on the surface of topological interphase by XPS was carried out (Table S3, Supporting Information). The results show that the proportion of total F element (1.69 wt%) in the topological interphase is relatively small compared with that of topological polymer (C, 64.09 wt%; O, 24.62 wt%), which indicates that the main component of interphase is topological polymer (CPDOL-Li), so its high modulus mainly comes from the contribution of topological polymer. The above results can be explained that topological polymer-reinforced interphase composed of CPDOL-Li exhibits higher mechanical strength than that of interphase with linear polymer. The construction of topological interphase with high Young's modulus can help suppress undesirable Li dendrite growth at high areal current density, maintaining the integrity and stability of SEI layer during cycling.

The above characterizations prove that the topological interphase of CPDOL-Li can effectively reconcile the contradiction between mechanical strength and diffusion dynamics of Li^+, resulting in an interphase with both high mechanochemical stability and low activation energy. To further explain the principle of decoupling contradiction by topological design, the relationship between entropy and mechanical strength is presented below (Equation 1).[10,23]

$$F = -T\frac{dS(L)}{dL} = -kT\frac{d\ln\Omega(L)}{dL} \quad (1)$$

F is the external force, T is the temperature of the chain, S is the entropy, L is the same average length.

The entropy (S) of topological CPDOL-Li is high because the topological structures of CPDOL-Li have countless and variable configurations and sizes (e.g., cyclic and hyperbranched polymers), which are brought about by random radical polymerization. According to Equation (1), the mechanical strength (the external force, F) could be effectively enhanced in this high entropy system.[10] In addition, abundant −O− sites on dioxolane segment bring a superior environment for Li^+ dissociation, and the weak C=O− and −N− coordination bonds on methacrylate and urethane segments can effectively promote diffusion dynamics of Li^+ (Figure S22, Supporting Information).

2.3. Performance Evaluations of Symmetrical Cells with Topological Interphases

The formation of stable and fast ion transport pathways can be certified by observing the superior cycling performance of symmetric Li/CPDOL-SPE/Li cells. The galvanostatic cycles of symmetrical Li/Li cells were used to verify the cycling performance of CPDOL-based topological interphase and PDOL-based interphase (**Figure 4**a). Compared with the Li/Li cycling performance of previously reported solid electrolytes (Figure 4b, Table S4, Supporting Information), the Li/Li cell with CPDOL-SPE exhibits stable voltage profiles with a constant overpotential of ≈62 mV for more than 3000 h at operating temperature. In sharp comparison, the cell using PDOL-SPE renders fluctuant voltage profile with large overpotential exceeding 398 mV around 100 h, and eventually incurs internal short circuit at around ≈138 h caused by rapid lithium dendrite growth. Furthermore, to clarify the evolution of the SPE/Li interface, the impedance evolution of Li/Li symmetric cells at different cycles are illustrated (Figure S23a,b, Supporting Information) and listed (Table S5, Supporting Information). The R_{SEI} and R_{ct} of CPDOL-SPE-based cell stay stable (42 and 337 Ω) upon first few cycling, and gradually reduce to stable interface impedances of 44 and 300 Ω, indicating the formation of a topological interphase layer with low activation energy and high mechanochemical stability. In contrast, the R_{SEI} and R_{ct} of the PDOL-SPE counterpart are obviously larger (142 and 444 Ω) at initial cycling and continuously greatly increase upon cycling (196 and 731 Ω at 20 h) (Figure 4c), indicating the appearance of serious side reactions caused by unstable interphase. Additional Li/Li cycling tests at varied current densities show CPDOL-SPE-based cell can deliver stable cycling with an overpotential of ≈203 mV at a current density of 0.4 mA cm^{-2} (Figure 4d), in sharp contrast to the unstable behavior of the PDOL-SPE at a current of 0.4 mA cm^{-2}, exhibiting high electrochemical stability of topological interphase. Since the dendrite growth is related to the space charge at LMA caused by Li^+ depletion, prolonging Sand's time is a valid method to evaluate stability of interphase. For instance, PDOL-SPE experiences a divergence in voltage and then short circuit after 26 h of growth of dendrite, while the divergence time of CPDOL-SPE is more than 97 h, indicating a better ability to inhibit the penetration of lithium dendrites (Figure S24, Supporting Information). To evaluate lithium nucleation behaviors, varied Cu/Li cells were assembled. The Cu/Li cell using CPDOL-SPE delivers a stable coulombic efficiency exceeding 92% after 200 cycles, much higher and more stable than that of the Cu/PDOL-SPE/Li cell (Figure S25, Supporting Information). These findings indicate that the CPDOL-based SEI can induce homogeneous, reversible Li deposition/dissolution kinetics and meanwhile suppress Li dendrite growth, benefitted by the formation of topological interphase with low activation energy and high mechanical stability. Furthermore, the SEM images of cycled LMAs disassembled from the Li/Li batteries were also investigated. A smooth surface on the LMA without obvious cracks and pits after cycling is observed when using CPDOL-SPE (Figure 4e), while the anode surface of PDOL-SPE-based cell exhibits a pulverized rough surface with cracks and inhomogeneous Li deposition after cycling (Figure S26, Supporting Information). This result demonstrates that an intimate interphase is constructed, which enables the uniform deposition of Li^+. To further explore the origin of the stability of the as-designed topological interphase layers, XPS analyses of the cycled LMAs disassembled from Li/SPE/Li cells after 50 cycles were conducted. In the XPS C1s spectrum of CPDOL-based SEI, the peak of –C–N (≈287.2 eV) bond appears and the peak of decomposed –C–F bond (≈293.2 eV) is reduced compared to that of the PDOL-based SEI (Figure 4f).[24] In the XPS O1s spectrum, the SEI layer toward CPDOL-SPE shows reduced polymer decomposition component CO_3^{2-} (≈531.2 eV) and a slight decrease in –S=O (≈531.8 eV) than that of PDOL-SPE counterpart, which is also consistent with the results in the C1s spectrum (Figure 4g).[4a,25] These findings indicate that the formation of N-rich topological SEI can reduce the decomposition of solid electrolyte and LiTFSI, demonstrating the superior chemical stability of topological interphase. In addition, an enhanced LiF peak (≈685.1 eV) appears in the CPDOL-based SEI,[12a] which contrasts with that of PDOL-SPE counterpart, proving that the topological interphase can modulate homogeneous deposition of Li^+ ions flux on the surface of LMA and constructed a LiF-rich SEI (Figure 4h). The abovementioned researches on Li deposition behaviors and mechanical-chemical-electrical properties of formed SEI indicate the behaviors of dendrite-free, uniform, and reversible Li deposition brought by the generation of topological interphase, confirming the effectiveness of the decoupling strategy.

2.4. Performance Evaluations of SSLMBs with Topological Interphases

To verify the utility of in situ topological interphases, 4 V $LiFePO_4$/Li SSLMBs were assembled and evaluated. As shown in **Figure 5**a, the resulting battery of long-term cycling at 0.25 C achieves a high initial discharge capacity of 158.6 mAh g^{-1} after activation, and exhibits a high capacity retention of 90.5% after 400 cycles at an operation time exceeding 3800 h. In sharp contrast, the battery using PDOL-SPE delivers a lower initial discharge capacity of 147.7 mAh g^{-1} and fluctuation of coulombic efficiencies owing to low ionic conductivity and the formation of an undesirable SEI. This undesirable SEI results in sluggish Li^+ transport kinetics, increased overpotential, and

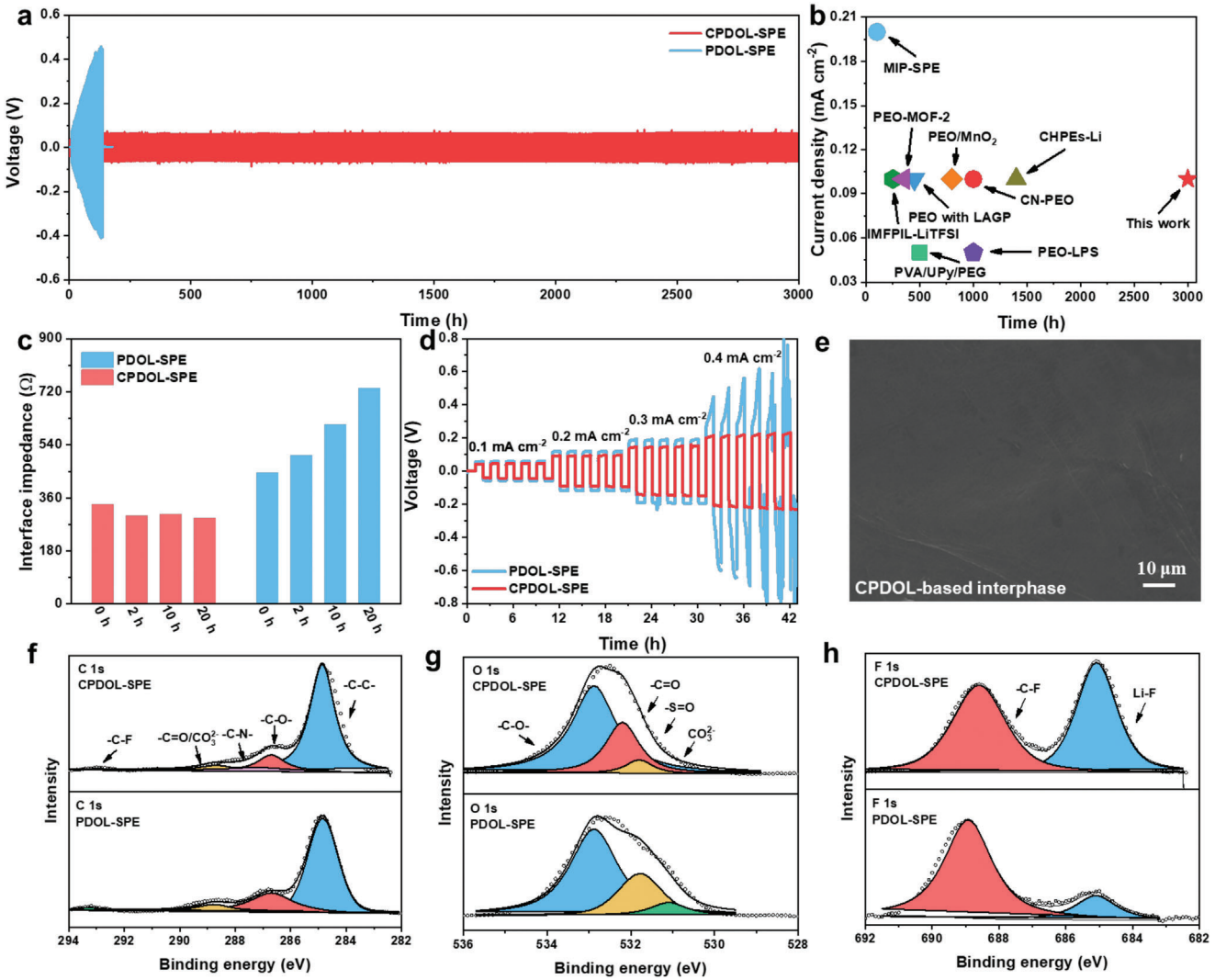

Figure 4. Performance of Li/Li symmetric cells with topological solid electrolyte interphase (SEI) layers. a) Voltage profiles of the Li/Li symmetric cells using cross-linked poly(1,3-dioxolane)-based solid-polymer-electrolyte (CPDOL-SPE) and PDOL-SPE at 0.1 mA cm^{-2} and 0.1 mAh cm^{-2}. b) Comparison of the cycle life of symmetric cells with CPDOL-SPE and those of previously reported excellent SPEs at 60 °C. PEO with LAGP,[26] MIP-SPE,[27] PEO/MnO,[28] PVA/UPy/PEG,[29] IMFPIL-LiTFSI,[30] CHPEs-Li,[31] PEO-LPS,[32] CN-PEO,[33] PEO-MOF-2.[34] c) Fitting results of interface impedances of Li/Li cells assembled with CPDOL-SPE and PDOL-SPE at different cycles. d) Voltage profile of Li/Li symmetric cells with CPDOL-SPE and PDOL-SPE charged and discharged for 1 h at various current densities. e) Top-view image of CPDOL-based SEI after 50 cycles. f) XPS spectra of C 1s of cycled CPDOL-based SEI and PDOL-based SEI. g) XPS spectra of O 1s of cycled CPDOL-based SEI and PDOL-based SEI. h) XPS spectra of F 1s of cycled CPDOL-based SEI and PDOL-based SEI.

eventually causes capacity fading with a lower capacity retention of 80.7% after 300 cycles (Figure 5b and Figure S27a, Supporting Information). Impressively, the long-term cycling performance of $LiFePO_4$/CPDOL-SPE/Li battery under higher current density and practical conditions is also much more stable than that of the PDOL-SPE counterpart. The as-prepared $LiFePO_4$/100 μm Li metal battery with CPDOL-SPE demonstrates a high discharge capacity retention of 95.1% (116.5 mAh g^{-1}) of the initial capacity with a high average coulombic efficiencies exceeding 99.78% at 0.5 C after 500 cycles (Figure 5c). It is worth noting that the specific capacity of CPDOL-based cell decreases after experiencing an unexpected sharp drop in temperature, but the specific capacity and coulombic efficiency quickly returned to normal after the temperature returned to normal, indicating that CPDOL-SPE with topological interphase has the potential to be used at lower temperatures and exhibits excellent reversibility. By contrast, $LiFePO_4$/PDOL-SPE/Li battery experiences rapid capacity fade from the initial cycle and fluctuation of coulombic efficiencies due to interphase instability at high current and the continuous consumption of lithium under practical condition during cycling (Figure 5c and Figure S27b, Supporting Information). Compared with the cycling performance of previously reported solid electrolytes (Table S6, Supporting Information), CPDOL-SPE has relatively good performance, and its superior cyclability together with higher coulombic efficiency enabled by using CPDOL-SPE can be interpreted as the formation of a

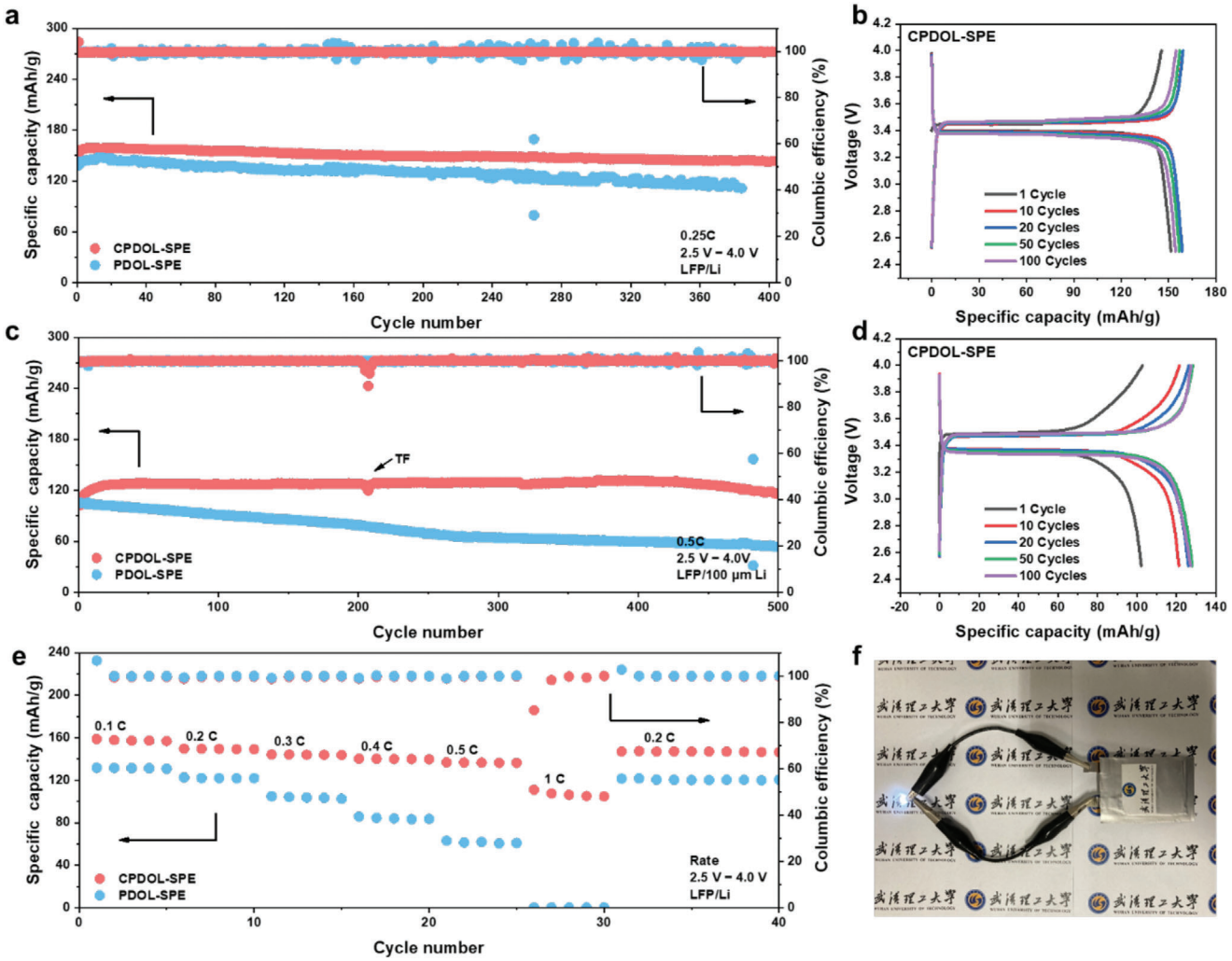

Figure 5. Performance of solid-state lithium metal batteries (SSLMBs) with topological solid electrolyte interphase (SEI) layers. a) Cycling performance of $LiFePO_4$/Li at 0.25 C. b) The corresponding charge/discharge profiles at different cycles of the cross-linked poly(1,3-dioxolane)-based solid-polymer-electrolyte (CPDOL-SPE) based $LiFePO_4$/Li cell. c) Cycling performance of $LiFePO_4$/100 μm Li at 0.5 C. Temperature fluctuation (TF), thermal insulation system failed for 1 d. d) The corresponding charge–discharge profiles at different cycles of the CPDOL-SPE-based $LiFePO_4$/100 μm Li cell. e) Rate performance of $LiFePO_4$/Li cells at different rates. f) Optical photograph of the $LiFePO_4$/CPDOL-SPE/Li pouch battery at room temperature.

topological SEI with functions of mechanochemical stability and fast ion transport, which can also be supported by the obviously lower battery polarization during cycling (Figure 5d). Moreover, the rate performance of the corresponding $LiFePO_4$/Li metal battery was measured from 0.1 to 1 C. For instance, the battery with CPDOL-SPE can still charge and discharge stably under 1 C rate (a specific discharge capacity of 107.5 mAh g^{-1}), and can well turn back to the initial discharge capacity at 0.1 C (a specific discharge capacity of 147.4 mAh g^{-1}) (Figure 5e). While the battery using PDOL-SPE demonstrates low specific discharge capacity at low rates and cannot be discharged at 1 C rate. These results show that CPDOL-SPE-based cell with topological interphase exhibits stable capability of high-current charging and discharging and ability of high reversibility. For practical safety evaluation, the $LiFePO_4$/CPDOL-SPE/Li pouch battery was assembled to test. This pouch battery enables the white LED device (exceeding 3.4 V) to work properly (Figure 5f) even after being cut in half (Figure S28, Supporting Information), showing the potentially high safety of CPDOL-SPE-based SSLMBs. These results mentioned above clearly indicate that CPDOL-SPE can endow high-current SSLMB with superior cycling stability and high safety, showing good potential for practical implementation.

3. Conclusion

In this work, a well-designed CPDOL-SPE that can in situ construct a topological interphase layer is developed to reconcile the contradiction between mechanical strength and the interphase activation energy of Li^+ transport. The synthesized CPDOL-SPE delivers excellent electrochemical properties such as high ionic conductivity, high $t_{Li}{}^+$, and high oxidation stability, showing great potential for battery applications. Moreover, the as-formed topological interphase layer exhibits fast diffusion dynamics of Li^+, suppression of cracks of SEI layer, and effective prohibition of

further side reactions. As a result, the as-developed symmetrical cell with CPDOL-SPE can deliver stable Li plating/stripping behaviors exceeding 3000 h at a current density of 0.1 mA cm^{-2}. Furthermore, 95.1% capacity retention of CPDOL-SPE-based cell beyond 500 cycles with $LiFePO_4$ cathode and practical LMA is also achieved. The design strategy to achieve topological interphase layer provides a promising route for practical realization of long-life SSLMBs.

Supporting Information

Supporting Information is available from the Wiley Online Library or from the author.

Acknowledgements

This work was supported by the National Key Research and Development Program of China (2020YFA0715000), the National Natural Science Foundation of China (52272234, 52127816), the Key Research and Development Program of Hubei Province (2021BAA070), Independent Innovation Project of the Hubei Longzhong Laboratory (2022ZZ-20), and Sanya Science and Education Innovation Park of Wuhan University of Technology (2021KF0011).

Conflict of Interest

The authors declare no conflict of interest.

Data Availability Statement

The data that support the findings of this study are available from the corresponding author upon reasonable request.

Keywords

lithium metal anodes, poly-dioxolane, solid electrolyte interfaces, solid-state electrolytes, topological interphases

Received: December 29, 2022
Revised: March 25, 2023
Published online:

[1] a) S. Randau, D. A. Weber, O. Kötz, R. Koerver, P. Braun, A. Weber, E. Ivers-Tiffée, T. Adermann, J. Kulisch, W. G. Zeier, F. H. Richter, J. Janek, *Nat. Energy* **2020**, *5*, 259; b) D. Lei, K. Shi, H. Ye, Z. Wan, Y. Wang, L. Shen, B. Li, Q.-H. Yang, F. Kang, Y.-B. He, *Adv. Funct. Mater.* **2018**, *28*, 1707570; c) S. Bag, C. Zhou, P. J. Kim, V. G. Pol, V. Thangadurai, *Energy Storage Mater.* **2020**, *24*, 198; d) A. A. Bristi, A. J. Samson, A. Sivakumaran, S. Butler, V. Thangadurai, *ACS Appl Energy Mater* **2022**, *5*, 8812.

[2] a) H. Xu, H. Zhang, J. Ma, G. Xu, T. Dong, J. Chen, G. Cui, *ACS Energy Lett.* **2019**, *4*, 2871; b) H. Zhang, L. Huang, H. Xu, X. Zhang, Z. Chen, C. Gao, C. Lu, Z. Liu, M. Jiang, G. Cui, *eScience* **2022**, *2*, 201; c) M. Yang, L. Chen, H. Li, F. Wu, *Energy Mater. Adv.* **2022**, *2022*, 9842651; d) T.-F. Yi, J.-J. Pan, T.-T. Wei, Y. Li, G. Cao, *Nano Today* **2020**, *33*, 100894.

[3] a) Y. Lu, C.-Z. Zhao, H. Yuan, X.-B. Cheng, J.-Q. Huang, Q. Zhang, *Adv. Funct. Mater.* **2021**, *31*, 2009925; b) K. Yang, L. Chen, J. Ma, C. Lai, Y. Huang, J. Mi, J. Biao, D. Zhang, P. Shi, H. Xia, G. Zhong, F. Kang, Y.-B. He, *Angew. Chem., Int. Ed.* **2021**, *60*, 24668; c) D. Zhang, M. Liu, J. Ma, K. Yang, Z. Chen, K. Li, C. Zhang, Y. Wei, M. Zhou, P. Wang, Y. He, W. Lv, Q.-H. Yang, F. Kang, Y.-B. He, *Nat. Commun.* **2022**, *13*, 6966.

[4] a) R. Hu, H. Qiu, H. Zhang, P. Wang, X. Du, J. Ma, T. Wu, C. Lu, X. Zhou, G. Cui, *Small* **2020**, *16*, 1907163; b) S. Sarkar, B. Chen, C. Zhou, S. N. Shirazi, F. Langer, J. Schwenzel, V. Thangadurai, *Adv. Energy Mater.* **2023**, *13*, 2203897; c) S. Sarkar, V. Thangadurai, *ACS Energy Lett.* **2022**, *7*, 1492.

[5] a) D. Chen, S. Huang, L. Zhong, S. Wang, M. Xiao, D. Han, Y. Meng, *Adv. Funct. Mater.* **2020**, *30*, 1907717; b) S. Tan, Y. Jiang, S. Ni, H. Wang, F. Xiong, L. Cui, X. Pan, C. Tang, Y. Rong, Q. An, *Natl. Sci. Rev.* **2022**, *9*, nwac183.

[6] a) L. Li, W. Liu, H. Dong, Q. Gui, Z. Hu, Y. Li, J. Liu, *Adv. Mater.* **2021**, *33*, 2004959; b) K. Ma, B. Chen, C.-X. Li, V. Thangadurai, *J. Phys. Chem. C* **2022**, *126*, 7828; c) V. Thangadurai, B. Chen, *Chem. Mater.* **2022**, *34*, 6637.

[7] a) R. Lin, Y. He, C. Wang, P. Zou, E. Hu, X.-Q. Yang, K. Xu, H. L. Xin, *Nat. Nanotechnol.* **2022**, *17*, 768; b) X. Meng, K. C. Lau, H. Zhou, S. K. Ghosh, M. Benamara, M. Zou, *Energy Mater. Adv.* **2021**, *2021*, 9786201.

[8] M. Arrese-Igor, M. Martinez-Ibañez, E. Pavlenko, M. Forsyth, H. Zhu, M. Armand, F. Aguesse, P. López-Aranguren, *ACS Energy Lett.* **2022**, *7*, 1473.

[9] G. G. Eshetu, X. Judez, C. Li, O. Bondarchuk, L. M. Rodriguez-Martinez, H. Zhang, M. Armand, *Angew. Chem., Int. Ed.* **2017**, *56*, 15368.

[10] Y. Su, X. Rong, H. Li, X. Huang, L. Chen, B. Liu, Y. S. Hu, *Adv. Mater.* **2023**, *35*, 2209402.

[11] F. A. Soto, A. Marzouk, F. El-Mellouhi, P. B. Balbuena, *Chem. Mater.* **2018**, *30*, 3315.

[12] a) Q. Zhao, X. Liu, S. Stalin, K. Khan, L. A. Archer, *Nat. Energy* **2019**, *4*, 365; b) H. Yang, B. Zhang, M. Jing, X. Shen, L. Wang, H. Xu, X. Yan, X. He, *Adv. Energy Mater.* **2022**, *12*, 2201762.

[13] W. Li, J. Gao, H. Tian, X. Li, S. He, J. Li, W. Wang, L. Li, H. Li, J. Qiu, *Angew. Chem., Int. Ed.* **2022**, *61*, e202114805.

[14] K. M. Diederichsen, E. J. McShane, B. D. McCloskey, *ACS Energy Lett.* **2017**, *2*, 2563.

[15] W. Chen, S. Li, C. Wang, H. Dou, X. Zhang, *Energy Environ. Mater.* **2022**, https://doi.org/10.1002/eem2.12412.

[16] J. N. Chazalviel, *Phys. Rev. A* **1990**, *42*, 7355.

[17] T. Zhou, Y. Zhao, M. El Kazzi, J. W. Choi, A. Coskun, *ACS Energy Lett.* **2021**, *6*, 1711.

[18] T. Lu, F. Chen, *J. Comput. Chem.* **2012**, *33*, 580.

[19] G. Merino, A. Vela, T. Heine, *Chem. Rev.* **2005**, *105*, 3812.

[20] X. Li, X. Han, H. Zhang, R. Hu, X. Du, P. Wang, B. Zhang, G. Cui, *ACS Appl. Mater. Interfaces* **2020**, *12*, 51374.

[21] a) P. Zhou, Y. Xia, W.-h. Hou, S. Yan, H.-Y. Zhou, W. Zhang, Y. Lu, P. Wang, K. Liu, *Nano Lett.* **2022**, *22*, 5936; b) S. Kundu, W. Xia, W. Busser, M. Becker, D. A. Schmidt, M. Havenith, M. Muhler, *Phys. Chem. Chem. Phys.* **2010**, *12*, 4351; c) Y. Guo, P. Niu, Y. Liu, Y. Ouyang, D. Li, T. Zhai, H. Li, Y. Cui, *Adv. Mater.* **2019**, *31*, 1900342.

[22] a) J. Chen, Z. Yang, G. Liu, C. Li, J. Yi, M. Fan, H. Tan, Z. Lu, C. Yang, *Energy Storage Mater.* **2020**, *25*, 305; b) X. Shen, R. Zhang, X. Chen, X.-B. Cheng, X. Li, Q. Zhang, *Adv. Energy Mater.* **2020**, *10*, 1903645.

[23] Y. Matsushita, H. Momose, Y. Yoshida, I. Noda, *Polymer* **1997**, *38*, 149.

[24] H. Xu, C. Sun, S. Zhang, H. Zhang, Z. Liu, Y. Tang, G. Cui, *ChemSusChem* **2023**, 202202334.

[25] J. G. Castaño, C. Arroyave, M. Morcillo, *J. Mater. Sci.* **2007**, *42*, 9654.

[26] X. Wang, H. Zhai, B. Qie, Q. Cheng, A. Li, J. Borovilas, B. Xu, C. Shi, T. Jin, X. Liao, Y. Li, X. He, S. Du, Y. Fu, M. Dontigny, K. Zaghib, Y. Yang, *Nano Energy* **2019**, *60*, 205.

[27] J. Seo, G.-H. Lee, J. Hur, M.-C. Sung, J.-H. Seo, D.-W. Kim, *Adv. Energy Mater.* **2021**, *11*, 2102583.
[28] Y. Li, Z. Sun, D. Liu, Y. Gao, Y. Wang, H. Bu, M. Li, Y. Zhang, G. Gao, S. Ding, *J. Mater. Chem. A* **2020**, *8*, 2021.
[29] Y. H. Jo, B. Zhou, K. Jiang, S. Li, C. Zuo, H. Gan, D. He, X. Zhou, Z. Xue, *Polym. Chem.* **2019**, *10*, 6561.
[30] Y. Zhou, Y. Yang, N. Zhou, R. Li, Y. Zhou, W. Yan, *Electrochim. Acta* **2019**, *324*, 134827.
[31] C. Zuo, M. Yang, Z. Wang, K. Jiang, S. Li, W. Luo, D. He, C. Liu, X. Xie, Z. Xue, *J. Mater. Chem. A* **2019**, *7*, 18871.
[32] P. Mirmira, C. Fuschi, W. Gillett, P. Ma, J. Zheng, Z. D. Hood, C. V. Amanchukwu, *ACS Appl. Energy Mater.* **2022**, *5*, 8900.
[33] H. Liang, S. Wang, Q. Ye, C. Zeng, Z. Tong, Y. Ma, H. Li, *Chem. Commun.* **2022**, *58*, 10821.
[34] G. Lu, H. Wei, C. Shen, F. Zhou, M. Zhang, Y. Chen, H. Jin, J. Li, G. Chen, J. Wang, S. Wang, *ACS Appl. Mater. Interfaces* **2022**, *14*, 45476.